

Environment dependent vibrational heat transport in molecular Junctions : Rectification, quantum effects, vibrational mismatch

Jayasmita Behera and Malay Bandyopadhyay
SBS, I.I.T. Bhubaneswar, Argul, Jatni, Khurda, Odisha, India 752050.
(Dated: June 21, 2021)

Vibrational heat transport in molecular junctions is a central issue in different contemporary research areas like Chemistry, material science, mechanical engineering, thermoelectrics and power generation. Our model system consists of a chain of molecules which sandwiched between two solids that are maintained at different temperatures. We employ quantum self-consistent reservoir model, which is built on generalized quantum Langevin equation, to investigate quantum effects and far from equilibrium conditions on thermal conduction at nanoscale. The present self-consistent reservoir model can easily mimic the phonon-phonon scattering mechanisms. Different thermal environments are modelled as (i) Ohmic, (ii) sub-Ohmic, and (iii) super-Ohmic environment and their effects are demonstrated for the thermal rectification properties of the system with spring graded or mass graded feature. The behavior of heat current across molecular junctions as a function of chain length, temperature gradient and phonon scattering rate are studied. Further, our analysis reveals the effects of vibrational mismatch between the solids phonon spectra on heat transfer characteristics in molecular junctions for different thermal environments.

PACS numbers: 05.60.Gg, 02.70.-c, 63.22.+m, 44.10.+i, 44.05.+e

I. INTRODUCTION

In recent days a great amount of interest have been observed in the emerging field of molecular electronics with a focus on thermal transport through molecular junctions (MJs) using theoretical and experimental tools [1-6]. The low dimensional heat transport via phonons is a topic of a significant technological importance [7-10]. Typically our system consists of a chain of molecules bridging between two solids made of poorly electron-conducting components such as saturated hydrocarbons. Different atomic motions in the molecules (known as stretching mode) carry away thermal energy which they obtain through excited phonon modes in the contacts (solids) [11-13]. The focus of the present paper is thermal transport in molecules and different properties that control thermal conduction in molecular junctions [14-16]. This kind of studies have immense applications ranging from roughly atoms to large biological molecules [17-18], thermoelectric devices [19], control of charge transfer [20-22] and photothermal processes in biological systems [23]. Understanding of vibrational heat transport can provide useful information about the chemical reactivity of protein folding dynamics [18]. Furthermore, understanding thermal energy transport in low dimensional systems is essential for developing electronic, mechanical, thermal, and thermoelectric devices, specifically organic-inorganic heterostructures [24-26].

It is well known that quantum effects and anharmonic interactions play a vital role in vibrational heat transport. Particularly, these effects play a crucial role in thermal conductivity, thermalization process, development of Fourier's law, intra- and inter-molecular vibrational redistribution in short molecules, and in nonlinear and nonreciprocal effects [27-30]. But, it is a hefty task and a emerging research area to take into account

both quantum effect as well as anharmonic interaction in the simulation of vibrational heat transport in molecular junctions. Classical molecular dynamics simulation can easily take care of the anharmonic interaction but they are well above the quantum domain [31-33]. There are full quantum mechanical method based on Landauer formalism which only consider harmonic interaction [34-36]. Although nonequilibrium Green's function technique [37-40] and kinetic approaches can take into account anharmonic interactions but they are only applicable for systems with few quantum states or weak coupling limit or low anharmonicity. On the other hand, the Born-Oppenheimer principle [41], mixed quantum-classical technique [42], numerically exact path integral technique [43] can handle only certain models like spin-Boson model.

Considering both the anharmonic interaction (arising from phonon-phonon scattering) and quantum effects, our analysis is based on quantum self-consistent reservoir model (QSCRM) to test the problem of vibrational heat transport in a chain of atoms bridging between two solids that are maintained at different temperatures. Our model is based on chains of N beads and springs coupled to two solids at the edges, maintained at constant temperature differences. Each of the inner $(N - 2)$ beads are also connected to a self-consistent reservoir (SCR) (see Fig. 1). In this way the inner (self-consistent) baths introduce an effective way to provide a simple scattering mechanism that might lead to local equilibration and to the onset of the (diffusional) Fourier's law of heat conduction [2,13]. On the other hand, the temperature of these $(N - 2)$ internal baths is determined by demanding that there is no net heat flow between the chain atoms and the reservoirs at steady state.

The classical version of the QSCRM was introduced in Refs. [44-45]. Further, manifestation of Fourier's law and

development of local equilibrium in the thermodynamic limit are discussed in Refs. [46-47]. In the weak coupling limit the quantum version of this model was studied by Visscher and Rich [48]. Beyond the weak coupling limit the quantum version of this model was considered in the linear response regime by Dhar and Roy [49,50]. Beyond the linear-response approximation, Bandyopadhyay and Segal introduced an iterative numerical procedure for the QSCRM to examine the phenomenon of thermal rectification in short MJs [51]. Heat transport in graphene nanoribbons were studied using massive atomistic simulations of QSCRM in Ref. [52]. Recently, Fereidani and Segal used QSCRM to study quantum effects and vibrational mismatch in the context of vibrational heat transport in short MJs [53].

It has been confirmed by simulations, time resolved vibrational spectroscopy, and theoretical investigations that energy transfer from one chemical group to another in one direction is more facile than in the reverse direction [54], even if both chemical groups are excited to similar energy. One of the issues of the present paper is to address thermal transport and rectification in a chain of molecules bridging between two heat baths which may have different structure of spectrum. As an illustrative example one may think about PEG_4 oligomer bridging two moieties, which serve as heat baths (see Fig. 2). The coupling between the oligomer and the Bosonic reservoir can be characterized by different forms of the reservoir spectrum for distinct physical scenarios. The three main classes that are usually considered in the literature are the so-called Ohmic, sub-Ohmic and super-Ohmic spectra [55]. We will compare the thermalization process and rectification process for these three types of reservoirs. Understanding which type of environment is most suitable for rectification and thermalization process can be of great importance in the choice of the physical system in building different molecular devices [56]. Heat transport via a quasi-one-dimensional system, like carbon nanotubes shows anomalous transport [57]. Thus, investigating the effect of different thermal environment using typical systems is an important tool not only for theoretical development but also for future development of molecular devices.

Different aspects of quantum effects and anharmonicity in the thermal conduction of short molecules is demonstrated in a recent experiment [58]. In this experiment Majumdar et. al. considered a self-assembled monolayers of alkanes with about 10 methylene units which were sandwiched between metal leads with distinct phonon spectra characterized by different Debye frequencies [58]. By considering different solids, they also found that the thermal conductance decreased as the Debye-frequency mismatch between the two solids increased. Fascinated by this experimental results on phonon-mismatch and how quantum effects, anharmonicity, large temperature differences together with different thermal spectral densities play together to determine the thermal conductance of MJs — is another focus of the present paper.

Although the radiative contribution (photonic contribution) of heat transport in nanoscale can not be ignored. But, this photonic contribution of heat transport is completely out of scope in the present paper. We mainly concentrate on the phononic heat transport at nanoscale. But, one may go through Refs. [59-61] for recent developments in the radiative heat transport at nanoscale.

Having discussed this background, the rest of the paper is organized as follows. In Sec. II we present the QSCR model and describe the Physical entity. We further explain how to calculate the thermal properties of the model in the classical limit, in the linear response limit and in the quantum regime. Section III provides the heat current characteristics in different kind of systems, e.g., mass graded or spring graded domains, and manifest the onset of the thermal rectifying effect in an asymmetric setting for three different thermal environments. In Sec. IV, we study the thermal conductance of MJs with increasing molecular length, temperature, and phonon scattering rate for different spectral density of the environment. The combined effect of anharmonicity, quantumness, and phonon mismatch in thermal transport for the above mentioned three types of thermal environment are discussed in Sec. V. We discuss and conclude in Sec. VI.

II. MODEL HAMILTONIAN AND FORMALISM

In this section we describe our model system of linear chains which can represent oligomers, e.g., alkane chains [56], polyethylene glycol [62] molecules to calculate the vibrational heat current across MJs utilizing the QSCR technique. This technique is built on the generalized quantum Langevin equation and the steady-state properties can be calculated employing the Green's function formalism [19,43]. To take into account far from equilibrium situations in our model for heat transport, we adopt the numerical method introduced in Refs. [51,53]. In the present analysis we go beyond the method discussed in Refs. [51,53] and consider “structured” reservoirs with phonon spectra that are categorized as (i) Ohmic, (ii) sub-Ohmic and (iii) super-Ohmic. For comprehensiveness of the readers, we briefly describe the working equations of the QSCRM. We consider a one-dimensional (1D) chain with N particles connected by harmonic links. In the present paper we consider the problem of heat transfer in the quantum harmonic chain model with each inner site connected to a self-consistent (SC) reservoir. This model has been developed with the motivation to include nonlinear behavior in an effective way [44-46]. Each particle is bilinearly connected to an independent thermal reservoir. The temperature of the reservoirs attached to the first and last particles are set to T_1 and T_N , respectively. These two end reservoirs establish the boundary conditions and we refer them as “physical” reservoirs. We refer the inner $(N - 2)$ reservoirs as “self-consistent” (SC) reservoirs which introduces scattering effects without en-

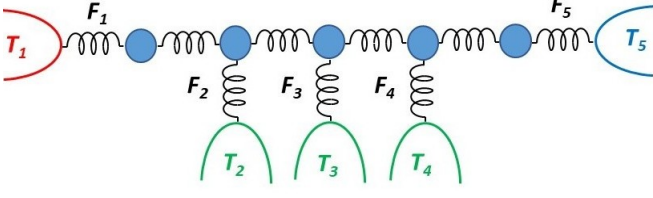


FIG. 1: Scheme of a chain of $N = 5$ particles; springs represent harmonic bond. The inner particles are connected to SC baths. The temperatures T_1 and T_5 sets the boundary conditions; the inner baths temperatures T_l are determined by demanding the leakage current $F_l = 0$. The net heat current flowing across the system is given by $F_1 = -F_5$.

ergy dissipation. The temperature of the SC reservoirs T_l ($l = 2, 3, \dots, N - 1$) are determined in a self-consistent manner by demanding that the net heat current between the chain atoms and the reservoirs is zero.

The Hamiltonian of the entire system consists of chain (S), left reservoir (L), right reservoir (R) and the inner baths (I) is given by harmonic potentials,

$$H = H_S + H_L + H_{LS} + H_R + H_{RS} + \sum_I H_I + \sum_I H_{IS}, \quad (1)$$

where

$$\begin{aligned} H_S &= \frac{1}{2} P_S^T M_S^{-1} P_S + \frac{1}{2} X_S^T K_S X_S, \\ H_B &= \frac{1}{2} P_B^T M_B^{-1} P_B + \frac{1}{2} X_B^T K_B X_B, \\ H_{BS} &= X_S^T K_{SB} X_B, \quad B = L, R, I. \end{aligned} \quad (2)$$

We use the index $B = L, R, I$ for different reservoirs and internal baths. The real diagonal matrices M_S and M_B represent the masses of the particles in the chain and in the reservoirs or baths, respectively. The force-constant matrices for the chain and reservoirs (baths) are given by the real symmetric matrices K_S and K_B , respectively. The term K_{SB} includes the force-constant coefficients between the chain and the baths. The column vectors X_S and X_B are the Heisenberg operators of the particles' displacements about some equilibrium positions with corresponding momenta operators P_S and P_B , respectively. The displacement operators and momenta operators satisfy the usual commutation relations $[X_l, P_m] = i\hbar\delta_{l,m}$ and $[X_l, X_m] = [P_l, P_m] = 0$. The Heisenberg equations of motion for the chain and the baths are given as follows:

$$M_S \ddot{X}_S = -K_S X_S - K_{SL} X_L - K_{SR} X_R - \sum_I K_{SI} X_I. \quad (3)$$

$$M_B \ddot{X}_B = -K_B X_B - K_{SB} X_S, \quad B = L, R, I. \quad (4)$$

Further, if we only consider a 1D chain with nearest

neighbor coupling, the Hamiltonian of the system is simplified as follows

$$H_S = \sum_{s=1}^N \frac{1}{2} m_s \dot{x}_s^2 + \sum_{s=1}^{N-1} \frac{1}{2} m_s \omega_0^2 (x_s - x_{s+1})^2, \quad (5)$$

where, force constant between the particles is given by $m_s \omega_0^2$ and the displacement from equilibrium of the s th particle is x_s .

Since the entire system is harmonic, the dynamics of the system can be written in terms of the generalized Langevin equation. After solving the Heisenberg equations of motion of the reservoir (Eq. (4)) and then plugging it back into Eq. (3) we obtain the generalized Langevin equation

$$\begin{aligned} m_s \ddot{x}_s(t) &= -m_s \omega_0^2 [2x_s(t) - x_{s-1}(t) - x_{s+1}(t)] \\ &\quad - \int_{-\infty}^t d\tau \dot{x}_s(\tau) \Gamma_s(t - \tau) + \eta_s(t), \quad s = 1, 2, \dots, N. \end{aligned} \quad (6)$$

The integral term in the equation (6) represents the dissipation of energy from the system to the environment and the last term is the fluctuating force of the bath acting on the system. The index s , labelling the friction kernel and the fluctuating force, can also be used to pin down the physical reservoirs or internal baths. The dynamical friction kernel can be written as $\Gamma_s(t - \tau) = 2\gamma_s f(t - \tau)$, where γ_s is the friction coefficient and $f(t - \tau)$ is memory function. We may consider $\Gamma_s(t - \tau) = 2\gamma_s \delta(t - \tau)$ for structureless and memoryless baths. To analyze the effect of vibrational mismatch on heat transport we use structured bath spectrum as follows [63]:

$$\Gamma_s(\omega) = \gamma_s \omega^{r-1} \exp\left(-\frac{|\omega|}{\omega_{d,s}}\right), \quad (7)$$

where, $r = 1$, $r < 1$ and $r > 1$ are characterized as Ohmic bath, sub-Ohmic bath, and super-Ohmic bath, respectively. For baths without exponential cut-off one can use $\omega_d \rightarrow \infty$ and for the exponential cut-off we may choose $\omega_d \sim \omega_0$ with $m = 1$. The frequency coefficient γ_s has different role for the physical and the SC reservoirs. $\gamma_{L,R}$ represent the bond energy of the molecule to the physical solids. On the other hand, γ_I ($I = 2, 3, \dots, (N - 1)$) denotes the effective anharmonicity in the system and it is usually interpreted as intramolecular vibrational relaxation rate. Usually the effect of phonon-phonon scattering is strong when γ_I is large and it reduces to harmonic limit when $\gamma_I = 0$. For simplicity, we consider constant value of γ_I . In the frequency domain, the dissipation and fluctuation force satisfy ($k_B = 1$)

$$\begin{aligned} &\frac{1}{2} \langle \eta_s(\omega) \eta_m(\omega') + \eta_s(\omega') \eta_m(\omega) \rangle \\ &= \frac{\hbar\omega}{2\pi} \Gamma_s(\omega) \coth\left(\frac{\hbar\omega}{2T_s}\right) \delta(\omega + \omega') \delta_{s,m}. \end{aligned} \quad (8)$$

The steady-state heat current at each bath can be obtained from the position-momentum correlation function

[64]. The phonon heat current towards the s th bead from the attached bath is given by

$$F_s = \sum_{m=1}^N \int_{-\infty}^{\infty} d\omega \Gamma_s(\omega) \Gamma_m(\omega) |[G(\omega)]_{s,m}|^2 \frac{\hbar\omega^3}{\pi} \times [f(\omega, T_s) - f(\omega, T_m)]. \quad (9)$$

This multi-terminal transport expression represents incoming energy from the s th particle to any of the other terminals and is termed as the ‘‘QSCR result.’’ Here the phonon Greens’ function, $G(\omega)$, is the inverse of a tridiagonal matrix with off-diagonal elements $-m_s\omega_0^2$, diagonal elements $2m_s\omega_0^2 - m_s\omega^2 - i\omega\Gamma(\omega)$, and $f(\omega, T) = [e^{\hbar\omega/T} - 1]^{-1}$ denotes the Bose-Einstein distribution function at temperature T . The temperature profile across the system is obtained by demanding that there is zero energy leakage from the system toward each of the SC baths,

$$F_i = 0, \quad i = 2, 3, \dots, N - 1. \quad (10)$$

Equation (10) gives $N - 2$ nonlinear equations which can be solved numerically (see Appendix A for details). The roots of the equation give the temperatures of the SC baths. Substituting these temperatures into the expression for F_1 (or equivalently, into F_N) gives the steady-state net heat current flowing across the system, $J = F_1 = -F_N$.

The QSCR is also applicable to obtain the behavior of heat current in the Quantum Linear-Response (QLR) regime and in the classical (C) domain.

In the linear response regime when the temperature difference along the chain is small, $(T_L - T_R)/T_a \ll 1$, where $T_a = (T_L + T_R)/2$, the differences in Bose-Einstein function $(f_s - f_m)$ in Eq. (9) can be Taylor expanded to $(T_s - T_m) \times \partial f / \partial T_a$. The QLR expression for heat current is now reduces to a linear expression,

$$F_s^{QLR} = \sum_{m=1}^N \int_{-\infty}^{\infty} d\omega \Gamma_s(\omega) \Gamma_m(\omega) |[G(\omega)]_{s,m}|^2 \frac{\hbar\omega^3}{\pi} \times \frac{\hbar\omega}{4T_a^2} \text{csch}^2 \left(\frac{\hbar\omega}{2T_a} \right) (T_s - T_m). \quad (11)$$

Similarly, in the classical domain we consider high temperature limit, $f(\omega, T) \sim T/(\hbar\omega)$, thus Eq. (9) reduces to

$$F_s^C = \sum_{m=1}^N \int_{-\infty}^{\infty} d\omega \Gamma_s(\omega) \Gamma_m(\omega) |[G(\omega)]_{s,m}|^2 \frac{\omega^2}{\pi} (T_s - T_m). \quad (12)$$

Since equations (11) and (12) are linear in SC baths temperatures, we can organize these equations as $F_s = \sum_m C_{s,m}(T_s - T_m)$, where $C_{s,m}$ contains the frequency integration. The solution for the temperature profile of the SC bath, demanding $F_s = 0$ for $s = 2, 3, \dots, N - 1$, is given by $\mathbf{T} = A^{-1}\mathbf{v}$ [49]. Here A is a $(N - 2) \times (N - 2)$

diagonal matrix with diagonal elements $\sum_{m \neq s} C_{s,m}$ and nondiagonal elements $-C_{s,m}$. \mathbf{v} is a vector defined as $v_s = C_{s,1}T_1 + C_{s,N}T_N$. The vector \mathbf{T} includes the steady-state temperatures of the inner baths. The net heat current F_1 can be readily calculate from the vector \mathbf{T} .

A. Physical Entity

We now try to express our simulation results in terms of physical units. As we are interested to tally our results for alkane chains, we may consider a mode of frequency 1000 cm^{-1} for the single bond carbon-carbon stretching motion. This translates into a frequency of $\omega_0 \sim 3 \times 10^{13} \text{ Hz}$. The other parameters which are used in the simulation are $T_a \sim 1$, $\gamma_{L,R} = 0.2$, $\gamma_I = 0.8$, and $\Delta T = 0.8$. As a result one can obtain heat current $J \sim 0.02 - 0.04$ for a chain length with $N \sim 6 - 12$ particles. Based on $\omega_0 \sim 3 \times 10^{13} \text{ Hz}$, one can obtain $T_a = 230 \text{ K}$, $\Delta T = 180 \text{ K}$ (figure 4 of Ref. [56]), $\hbar\gamma_{L,R} = 4 \text{ meV}$ for the molecule-surface contact energy and $\hbar\gamma_I = 16 \text{ meV}$ for the vibrational energy of scattering or 25 ps for scattering rate. Thus the heat current translates as $J \sim 2 \times 10^{-9} - 4 \times 10^{-9} \text{ W}$. Furthermore, one may calculate the thermal conductance which is given by $K_T = J/\Delta T = 14 - 20 \text{ pW/K}$ and it is comparable to experimental results on alkane chains with $4 - 20$ units [58].

We furthermore consider Debye solids and other kind of environmental spectrum with characteristic frequencies in the range of $0.1 - 1$, in units of ω_0 and it changes to $\omega_d = 3 \times 10^{12} - 3 \times 10^{13} \text{ Hz}$. If we consider Debye temperature, these numbers actually translates to $T_D = 22 - 220 \text{ K}$. Thus, this paper will enable us to implement a feasible technique to simulate quantum heat transport in molecular junctions.

III. RECTIFICATION

In the last decade, we have seen a large number of studies on thermal rectification which is nothing but an asymmetry of the heat current for forward and reverse temperature gradient [65]. It is usually seen that a well behaved rectifier acts as a heat conductor in one direction of temperature bias and it behaves as an insulator for the opposite direction of bias. It is well known that junctions which may incorporate an effective anharmonicity in the system with some sort of spatial asymmetry may demonstrate rectification [66]. Further, the self-consistent reservoirs include anharmonicity to the system in an effective way and it is useful to explore its rectification properties when we incorporate spatial asymmetry either by using spring graded chain (Fig. 3) or by using a mass graded chain (Fig. 6). The study on classical SC model and quantum linear-response (QLR) SC model prove that they will never show any kind of rectification even with the inclusion of spatial asymmetry [49]. Further studies reveal that full quantum treatment of the

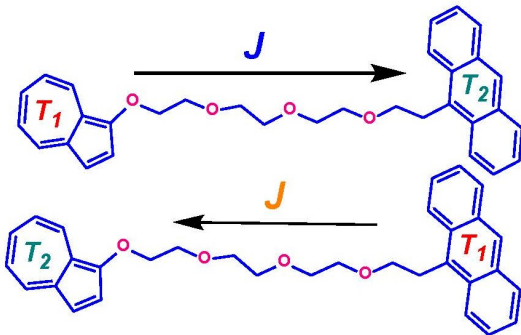


FIG. 2: Heat current flow through PEG_4 oligomer bridging two moieties (heat baths) for forward and reverse temperature gradient. Here $T_1 > T_2$.

QSCR model exhibit rectification [51]. But the effect of structured bath on the heat rectification is still open. In this section we study the rectification effect for both spring graded and mass graded chain systems for three different types of environment i.e., Ohmic, sub-Ohmic, and super-Ohmic environment. The bath spectrum is already defined in Eq. (7). We study the extent of rectification from the rectification ratio (R) which is defined as follows

$$R = \frac{J_+ - J_-}{(J_+ + J_-)}, \quad (13)$$

where J_+ and J_- are the absolute value of heat current for forward ($T_1 > T_N$) and reversed ($T_N > T_1$) temperature biases, respectively.

A. Spring graded system

We use the QSCR method for the spring graded system with variable force constant to study the rectification effect. Using a non-equilibrium molecular dynamics (MD) simulation of single walled carbon nanotube (SWNT)

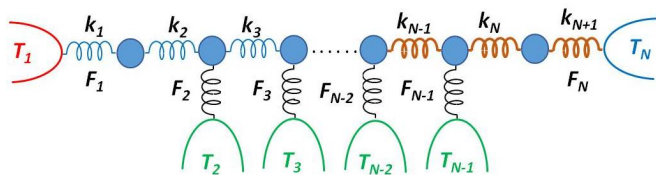


FIG. 3: A scheme of Spring graded system with SC baths for N particles. The spring graded system is described by dividing the system into two halves with both halves having different values of spring constants. Each half have identical value of spring constants. The two halves are shown by different color springs on both sides of the system separated by the dotted line.

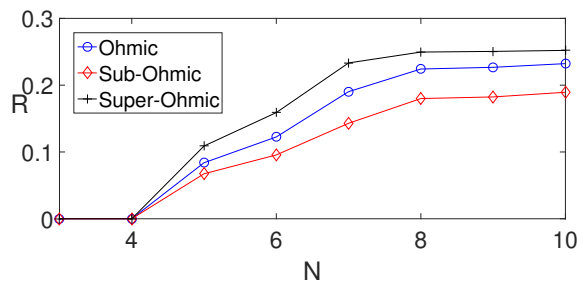


FIG. 4: Rectification in a spring graded system: Rectification ratio as a function of chain size for Ohmic (o), sub-Ohmic (◇), and super-Ohmic (+) environments. Parameters are $\gamma_0 = 0.2$ for all sites, $k_i = 1$, for $i = 1, 2, \dots, 5$ and $k_i = 4$ for $i = 6, 7, \dots, (N + 1)$. In the forward direction we used $\beta_1 = 1, \beta_N = 5$. Here $\beta \equiv 1/T$ is the inverse temperature. The temperature difference $\Delta T = T_1 - T_N = 0.8$. The average temperature $T_a = (T_1 + T_N)/2 = 0.6$. The temperatures of left and right reservoir are interchanged in reverse direction.

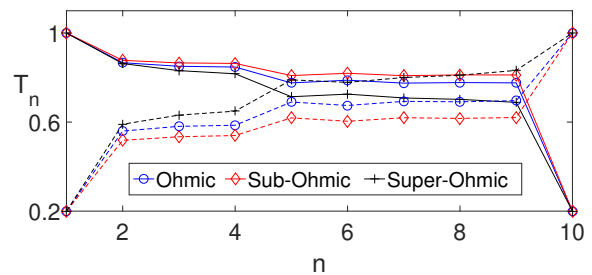


FIG. 5: Temperature profile at site n for a spring graded $N = 10$ chain in forward direction (solid line) and in reverse direction (dashed line) for Ohmic (o), sub-Ohmic (◇), and super-Ohmic (+) environments. Parameters are $\gamma_0 = 0.2$ for all sites, $k_i = 1$, for $i = 1, 2, \dots, 5$ and $k_i = 4$ for $i = 6, 7, \dots, (N + 1)$. In the forward direction we used $\beta_1 = 1, \beta_N = 5$. Here $\beta \equiv 1/T$ is the inverse temperature. The temperature difference $\Delta T = T_1 - T_N = 0.8$. The average temperature $T_a = (T_1 + T_N)/2 = 0.6$. The temperatures of left and right reservoir are interchanged in reverse direction.

people have investigated the defect-induced thermal rectification [67]. Hayashi et. al. [67] considered vacancy defects only in half of the region along the axial direction. Their results confirm that heat flow from the defective SWNT to the pristine SWNT is nearly 10% greater than in the opposite direction and it agrees with the experimental results of Wang et.al [68]. The defect is introduced by controlling the spring constant k_i . A defective SWNT has smaller number of sp^2 bonds which results in weaker interaction in the defect region with a smaller k value than the pristine region. We describe the spring graded system by dividing the system into two halves with both halves having different values of spring constants. Each half have identical value of spring constants. For a system of N particles we take $k_i = 1$ for $i = 1, 2, \dots, N/2$ and $k_i = 4$, for $i = N/2 + 1, \dots, (N + 1)$. For classical and QLR case the effect is negligible and one

may observe $J_+ \sim J_-$. On the other hand, for low temperatures and large bias, using QSCR method, one can demonstrate that J_+ and J_- deviate significantly. Figure 4 displays the plot of rectification ratio R with Chain size N for Ohmic, sub-Ohmic and super-Ohmic environments. Here we study a chain of $N = 10$ particles. We find that the rectification ratio increases with chain size and rectification is highest for super-Ohmic environment and least for sub-Ohmic environment.

B. Mass graded system

In the present subsection we demonstrate thermal rectification in an asymmetric quantum harmonic systems with SC baths by solving the set of nonlinear equations (9). We incorporate spatial asymmetry in QSCR model by using a mass graded system in which mass of the particles increases with the increase of chain size. However, as correctly pointed out in Ref. [69], most of the theoretical studies of heat rectification are based on the sequential coupling of two or three segments with different anharmonic potentials and they have following two drawbacks : (a) their experimental implementation are very much difficult and (b) the rectification power typically decays to zero with increasing the system size. Thus, people have

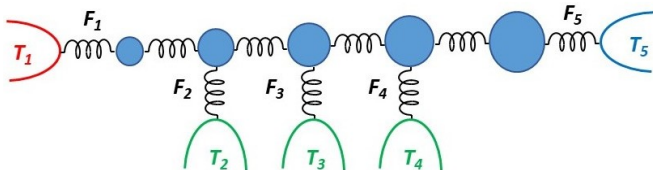


FIG. 6: A scheme of mass graded system with SC baths for $N = 5$ particles.

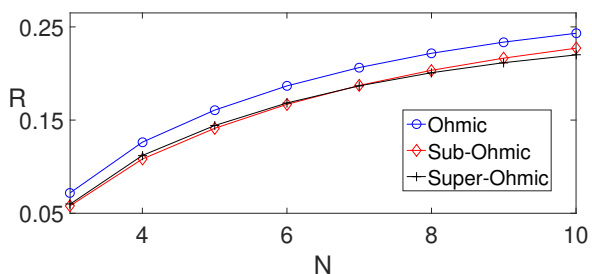


FIG. 7: Rectification in a mass graded system: Rectification ratio as a function of chain size for Ohmic (o), sub-Ohmic (\diamond), and super-Ohmic (+) environments, $\gamma_0 = 0.2$ for all sites, $M_1 = 0.2$, $M_n = M_1 + (n - 1) \times 0.2$. In the forward direction we used $\beta_1 = 1, \beta_N = 5$. Here $\beta \equiv 1/T$ is the inverse temperature. The temperature difference $\Delta T = T_1 - T_N = 0.8$. The average temperature $T_a = (T_1 + T_N)/2 = 0.6$. The temperatures of left and right reservoir are interchanged in reverse direction.

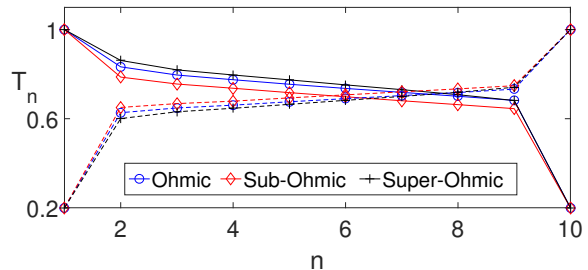


FIG. 8: Temperature profile at site n for a mass graded $N = 10$ chain in forward direction (solid line) and in reverse direction (dashed line) for Ohmic (o), sub-Ohmic (\diamond), and super-Ohmic (+) environments, $\gamma_0 = 0.2$ for all sites, $M_1 = 0.2$, $M_n = M_1 + (n - 1) \times 0.2$. In the forward direction we used $\beta_1 = 1, \beta_N = 5$. Here $\beta \equiv 1/T$ is the inverse temperature. The temperature difference $\Delta T = T_1 - T_N = 0.8$. The average temperature $T_a = (T_1 + T_N)/2 = 0.6$. The temperatures of left and right reservoir are interchanged in reverse direction.

found another way to produce the required asymmetry for thermal rectification by considering a mass gradient along the system length. This idea was first employed to experimentally build a rectifying device with a carbon and boron-nitride nanotube inhomogeneously mass-loaded with heavy molecules [70]. The experimental work with mass-loaded nanotubes was further numerically simulated (nonequilibrium molecular dynamics) by means of a one-dimensional (1D) Fermi–Pasta–Ulam (FPU) anharmonic oscillator lattice with a mass gradient [71–73]. Further theoretical studies on mass graded system can be found in Refs.[74–75].

With this background, we consider the force constant ($k = 1$) for all sites are equal. We take $M_1 = 0.2$ and $M_l = M_1 + 0.2 \times (l - 1)$ with $l = 2, 3, \dots, N$. Figure 7 displays the plot of rectification ratio with chain size for mass graded system with different environmental spectrum. While at high temperatures and for $T \ll T_a$ the effect is negligible and $J_+ \sim J_-$. On the other hand, J_+ and J_- deviates significantly at low temperatures and for large bias, with the current being larger in the direction of increasing masses. It is also seen that the rectification ratio increases with chain size, an observation that can be reasoned by the growing mass ratio along the chain. In order to better understand the mechanism of thermal rectification one can inspect the temperature profile for the rectifying system. One may observe a reflection symmetry of the temperature profile with respect to the average temperature at high temperatures, when the temperature bias is reversed [51]. Further we observe an asymmetry in the temperature profile in the deep quantum domain beyond linear response regime. The temperature gradient at the chain center is larger when the light masses are in contact with the hot bath than the gradient generated in the reversed case [51]. Furthermore, the asymmetry in the temperature profile of the Ohmic bath is larger compare to that of the sub-Ohmic and super-Ohmic cases.

This is reflected in the rectification plot (Figure 7) which shows largest rectification ratio for the Ohmic bath.

IV. HEAT TRANSPORT ACROSS MOLECULAR JUNCTION

In this section, we analyze the behavior of the heat current as a function of molecular length, temperature, and phonon-phonon scattering rate (γ_I). The main objective is to demonstrate that the QSCR method can reproduce qualitative behaviour of the heat transport across anharmonic molecular junctions (MJs). Although, the first-principle simulation results of quantum thermal conduction in anharmonic MJs are unavailable, but examination on heat transport in nanostructures [8-10], such as self-assembled monolayers, amorphous polymers, and nanowires, exhibit some typical features, like: (i) ballistic to diffusive transition dynamics and the recovery of the Fourier's law of thermal conduction with increasing length and (ii) the heat current as a function of temperature shows a turnover [6,53].

Further we make a comparative study on the heat transport across MJs based on the following three methods: (i) Using QSCR method we numerically solve Eqs. (9) and (10) and this nonlinear method enables us to catch far from equilibrium behaviour (large ΔT), effective anharmonicity (large γ_I), and quantum effects ($\hbar\omega_0/T_a > 1$) which is introduced through the Bose-Einstein statistics, (ii) In the small temperature gradient, one can use Quantum linear-response approximation with the help of Eq. (11), (iii) while using Eq. (12) one can obtain Classical limit results with the help of $T_a > \hbar\omega_0$.

Furthermore, we compare the results for each method for the three different bath spectrum: (i) Ohmic, (ii) Sub-Ohmic, (iii) Super-Ohmic environments.

A. Length dependence

In this subsection, we observe the behavior of the heat current with chain length which is displayed in Fig. 9 for short chain and Fig. 10 for long chain. The conductance of quantum harmonic systems for short molecules is usually make a non-monotonous behaviour with length [6, 28-30]. Furthermore, the heat current behaviour of such short molecules depend on the normal mode spectrum, temperature, the nature of the contacts, and the properties of the solids also dictate the heat current behaviour of such short molecules. Considering a 1-D ordered chain one can observe a ballistic behavior for harmonic systems. The QSCR method captures the anharmonic effect properly and it causes the decay of the current with molecular length, reflecting an increase in the thermal resistance. On the other hand, classical simulations always overestimate the current. In the quantum linear-response regime, the heat current is qualitatively close to the QSCR calculations.

Furthermore, one may find whether the SC reservoirs can reproduce Fourier's law of thermal conduction, i.e., $J \sim \frac{\Delta T}{N}$ [25]. One can observe that the temperature drop along the chain is relatively large for short molecules. As one increases the chain length one find that (inset) heat current behaviour approaches the Fourier's law $J \sim N^{-1}$. The QSCR method is computationally costly for large N . We perform the simulations for $N = 30$ to demonstrate the heat current behavior for long chain (see Fig. 10).

The behavior of heat current with chain length is displayed in figure 9 for different environmental spectrums. For short molecule the temperature drop along the chain is large. Here we examine whether the SC reservoirs can satisfy the Fourier's law of thermal conduction, i.e., $J \propto \frac{\Delta T}{N}$ [25]. For $N = 12$, a log-log plot of conductance length (see inset in Fig. 9(a)) reveals that the slope is same (~ -0.54) for both the Ohmic and sub-Ohmic cases whereas the slope is ~ -0.53 for the super-Ohmic environment. For $N = 30$ the log-log plot (see inset in

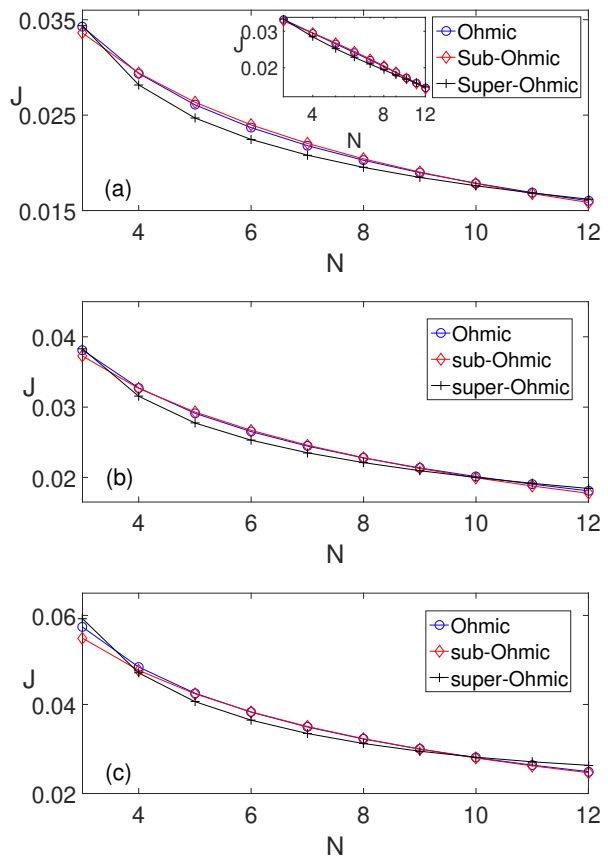


FIG. 9: Heat current as a function of chain size using the (a) QSCR method, (b) quantum linear-response, and (c) classical calculations for Ohmic (o), sub-Ohmic (\diamond), and super-Ohmic (+) environments. Parameters are $\beta_1 = 1$, $\beta_N = 5$, $\gamma_L = \gamma_R = 0.2$, $\gamma_I = 0.8$. Here $\beta \equiv 1/T$ is the inverse temperature. The temperature difference $\Delta T = T_1 - T_N = 0.8$. The average temperature $T_a = (T_1 + T_N)/2 = 0.6$. The inset in (a) displays the log-log scale plot.

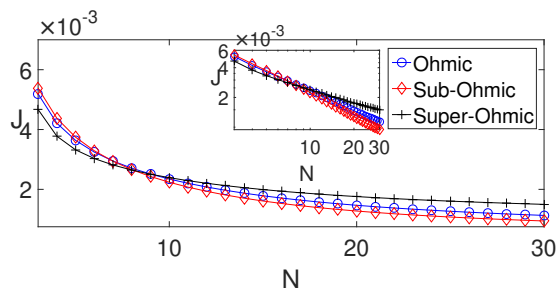


FIG. 10: Heat current as a function of chain size using the QSCR method for Ohmic (o), sub-Ohmic (\diamond), and super-Ohmic (+) environments. Parameters are $\beta_1 = 2$, $\beta_N = 4$, $\gamma_L = \gamma_R = 0.2$, $\gamma_I = 2$. Here $\beta \equiv 1/T$ is the inverse temperature. The temperature difference $\Delta T = T_1 - T_N = 0.25$. The average temperature $T_a = (T_1 + T_N)/2 = 0.375$. The inset displays the log-log scale plot.

Fig. 10) reveals that the slopes are ~ -0.66 , ~ -0.77 , and ~ -0.47 for the Ohmic, sub-Ohmic and super-Ohmic environment, respectively. Thus, we can conclude that the heat current reaches Fourier's law for the sub-Ohmic case with a shorter chain length compare to the other two. On the other hand, super-Ohmic environment requires largest chain length to attain Fourier's law.

B. Temperature dependence

We study the heat current as a function of temperature. The junction is biased following $T_{L,R} = T_a \pm \frac{\Delta T}{2}$. At low temperatures Classical results always exaggerate quantum simulations. On the other hand, QLR calculations may overestimate the QSCR results. Further, the simulation at high temperatures reveals that QSCR heat current saturates similar to harmonic predictions. The behavior of heat current with temperature is displayed in the Fig. 11. We see that at high temperature the results saturate for all the three environments. On the other hand, bulk [7] and nano-structure materials [70] typically

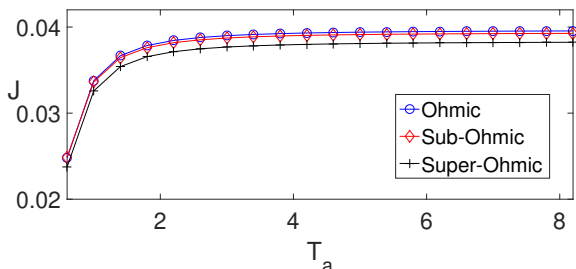


FIG. 11: Heat current as a function of average temperature using the QSCR method for Ohmic (o), sub-Ohmic (\diamond), and super-Ohmic (+) environments. Here $N = 10$, $\Delta T = 0.8$, $\gamma_L = \gamma_R = 0.2$. Temperature independent, $\gamma_I = 0.4$, phonon scattering rates.

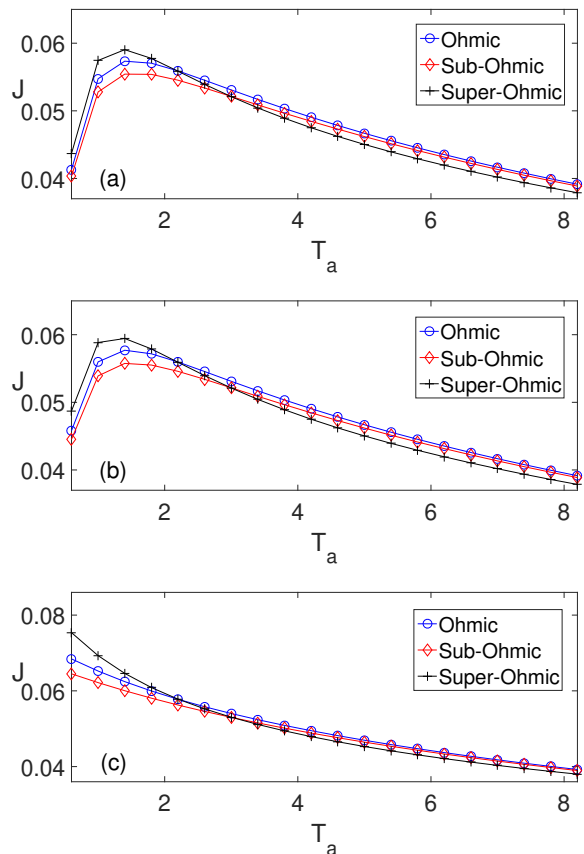


FIG. 12: Heat current as a function of average temperature using the (a) QSCR, (b) quantum linear-response, and (c) classical calculations for Ohmic (o), sub-Ohmic (\diamond), and super-Ohmic (+) environments. Here $N = 10$, $\Delta T = 0.8$, $\gamma_L = \gamma_R = 0.2$. Temperature dependent, $\gamma_I = 0.05T_a$, phonon scattering rates.

show a turnover behavior with temperature. The thermal conductance initially increases with T_a and it decays with T_a as one goes beyond $T_a \simeq \hbar\omega_0$ due to increasing significance of the (inelastic) Umklapp phonon-phonon scattering process. Hence, we can expect a significant role of anharmonic interactions in MJs as the temperature is increased. As we increase the temperature more number of modes become active and more pathways open up for the redistribution of vibrational energy which results in the increase of thermal resistance.

One can capture the turnover behavior in the QSCR method by making the internal scattering rates as a function of temperature, $\gamma_I(T_a) \propto T_a^p$, $p > 0$. This results in the increase of anharmonic effects as we increase the temperature, eventually suppress the current. Overall, the increase of γ_I with temperature leads to a turnover behavior. The turnover behavior for (a) QSCR, (b) quantum-linear response and (c) classical calculations for three different bath spectrum is shown in the Fig. 12. We see that the heat current increases for low temperature upto certain values of T_a and then decays for high tem-

perature limit in QSCRM and quantum-linear response case. However, the heat current decays for all temperature limits in classical calculation. When we consider temperature dependence of scattering rate, the heat current initially shoots up much more for the super-Ohmic environment than that of Ohmic and sub-Ohmic cases. This is quite different than that of temperature independent scattering rate (see Fig. 11). Above certain values of T_a , the heat current behaviour follows the usual decreasing nature where the decreasing rate is maximum for the super-Ohmic environment. Although, classical calculation is incapable to demonstrate such behaviour.

In the present study we consider $\gamma_I \propto T_a$ (with $p=1$) in consistency with the study of Refs.[16,53]. One can actually show that different scaling for the heat current with T_a can be achieved by adjusting the temperature dependence of the scattering rate. We examine a linear dependence. Further a study on quadratic form can be found in Ref.[53]. Although the later option is more physically imitates the phonon-phonon collision processes, as the occupation factor of each incoming phonon scales with temperature [53]. One can demonstrate a turnover behavior of the current with temperature around the same point for the both models, but they show distinct scaling laws. Therefore, by modifying the functional form $\gamma_I(T_a)$ (physically represents to different inter-molecular-vibrational rate) we can emulate different types of scattering processes.

C. Scattering rate dependence

It is well known that as we increase the scattering rates of the SC baths γ_I , it also increases the amount of anharmonicity in the model. The increase of γ_I ultimately enhances the phonon splitting and recombination processes. As a matter of fact the excitations are scattered between the SC baths, thus the thermal resistance grows with the increase of γ_I . Similar to earlier cases one may

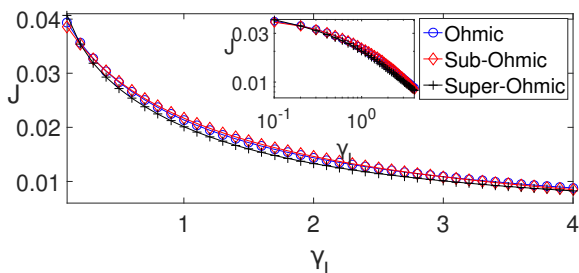


FIG. 13: Heat current as a function of phonon-phonon scattering rate γ_I using the QSCRM method for Ohmic (\circ), sub-Ohmic (\diamond), and super-Ohmic ($+$) environments. Here we take $N = 6, \beta_1 = 1, \beta_N = 5, \gamma_L = \gamma_R = 0.2$. Here $\beta \equiv 1/T$ is the inverse temperature. The temperature difference $\Delta T = T_1 - T_N = 0.8$. The average temperature $T_a = (T_1 + T_N)/2 = 0.6$.

observe that the heat current is escalated in the classical regime, and it is slightly overvalued in the QLR method. It is known from Refs. [51,53] that the thermal conductance is inversely proportional to the phonon scattering rate. But, the short molecules display deviation from this trend and it indicates that the current is dominated by the direct (harmonic) left-to-right transmission contribution. But, as we increase the chain length it approaches the theoretical limit. The effect of three different types of environment is quite similar in this perspective of scattering rate dependence (see Fig. 13).

Before concluding this section, we can summarize and explain all of our observed results of this section based on Kapitza resistance [76,77]. The interface thermal resistance (ITR) or the Kapitza resistance, measures the interfacial resistance to heat flow [76,77]. It is usually defined as $R = \frac{\Delta T}{J}$, where J is the heat flow (per unit area) and ΔT measures the temperature jump between two sides of the interface. The emergence of the Kapitza resistance can be thought of due to the heterogeneous vibrational properties of the two different materials fabricating the interface at which the energy carriers collide with each other. Usually the amount of relative transmission of heat energy banks on the available energy states on each of the two sides of the interface. It is observed that the ITR in our setup depends (a) on the direction of the applied temperature bias and (b) the degree of overlap of the power spectra between two segments i.e. the left (L) and right (R) segments of the interface. The underlying physical mechanism of the unsymmetrical ITR between two dissimilar segments at the interface can be connected to the match or mismatch of the corresponding power spectra. If the overlap of power spectra between two sectors is large one can expect large amount of heat flow along that interface and vice versa.

Let us first consider figure 12. As temperature increases, the power spectrum of the super-Ohmic bath shifts downward toward lower frequencies of the system and overlap or resonance of the spectrum between two sectors occur. In contrast, the power spectrum of the sub-Ohmic bath segment, however, shifts upward, toward higher frequencies. Because of these opposite shifts, overlap between power spectrum decreases and thermal energy flow is lesser than that of the super-Ohmic case. The same reasoning is applicable for Figure 14. Considering Figure 15 one can explain the phenomena as follows : one can think that the scattering effect is less available for the sub-Ohmic spectra and the overlap of power spectra across the interface is largest for the sub-Ohmic case. On the other hand, one can expect large amount of scattering for the super-Ohmic bath and the overlap is least for the super-Ohmic scenario.

V. PHONON MISMATCH: ENVIRONMENTAL EFFECT

In the previous section we have shown that the QSCR method is able to capture the anharmonic effects in quantum thermal transport. In the present section our focus is to study heat transport between two solid surfaces with structured and distinct phonon spectra. We use a simple model in which the phonon spectra are distinguished by an exponential cutoff frequency $\exp(-\omega/\omega_d)$, Eq. (7). Although we are using a simple set up but it is complex in nature as it includes the effect of anharmonicity, quantum effects, mismatched phonon spectra, and a far from equilibrium situation. The present section is devoted to study the effect of phonon mismatch between the two reservoirs on the heat current flow in MJs. The heat current usually drops as one increases the mismatch for a harmonic system but the inelastic scattering may help to tame it.

Here we are interested to study two cases: (a) exponential cut-off baths without mismatch, $\omega_{d,L} = \omega_{d,R}$, and (b) exponential cut-off baths with a vibrational mismatch, $\omega_{d,L} \neq \omega_{d,R}$. In Figure 14, we compare the result for the following three cases: (i) Ohmic, (ii) sub-Ohmic, and (iii) super-Ohmic environments. When we introduce vibrational mismatch, high frequency modes from left bath (hot) are barred to cross to the right cold bath unless and until energy is readjusted in the inner baths. But, the energy redistribution process is a slow method for short molecules and it results in suppression of heat current. Now, the dual role of SC reservoirs can be demonstrated. One can find that the increase of anharmonicity introduced by SC baths due to increase of phonon scattering rate γ_I increases the thermal resistance and thus reduces the current as shown in Fig. 13. On the other hand, the increase of inelastic scattering rate (γ_I) can be helpful to overcome vibrational mismatch. In Fig. 13, we observe that as we increase γ_I the heat current decreases. Further, if we consider Fig. 15 the situation is quite different for the vibrational mismatch. For small γ_I regime, as we increase the inelastic scattering rate the heat current increases. Thus the inelastic scattering is helping to overcome the vibrational mismatch in this regime. In this regime the anharmonicity is helpful in transport in the MJs. However, after reaching certain value of γ_I the SC baths increases the multiple scattering processes and dampen the heat current. The crossover between the two regimes depend on the length of the molecule (see Fig. 15). Further, one can observe that the effect is most prominent for the sub-Ohmic environment and least perceptible for the super-Ohmic case.

Next, we try to consider the experimental report in Ref. [58]. We consider molecular junctions with dissimilar phonon spectra at boundaries, captured by different Debye frequencies. We describe two such setups and study the heat current behavior with vibrational mismatch.

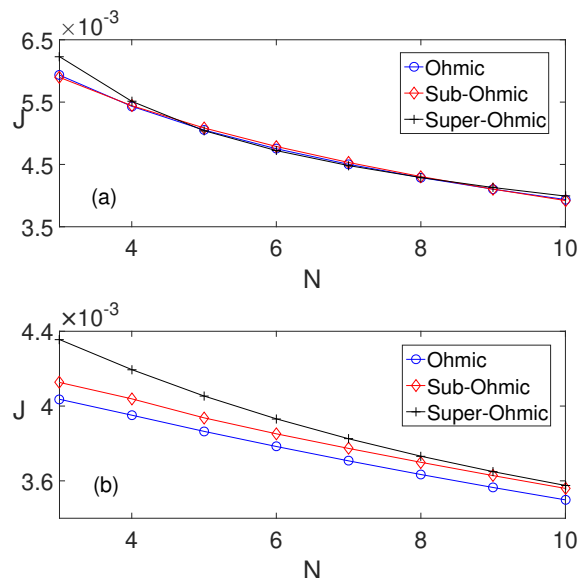


FIG. 14: Heat current as a function of chain length with (a) Debye baths without mismatch with $\omega_{d,L} = \omega_{d,I} = \omega_{d,R} = 4$, and (b) mismatched Debye baths with $\omega_{d,L} = 4, \omega_{d,I} = 1, \omega_{d,R} = 1$. In both the cases we use the QSCR method for Ohmic (o), sub-Ohmic (\diamond), and super-Ohmic (+) environments. We use $\beta_1 = 2, \beta_N = 4, \gamma_L = \gamma_R = 0.2, \gamma_I = 0.8$. Here $\beta \equiv 1/T$ is the inverse temperature, $\Delta T = 0.25$, $T_a = 0.375$.

A. Phonons up-conversion process

The cold bath is fixed with a Debye frequency of $\omega_{d,C} = 1$ as shown in Figure 16. The Debye frequency of the hot bath is gradually reduced, starting from the same value as the cold bath. In this setup, the collisions of phonons generate a high frequency mode (up-conversion) and it is helpful for transport. Figure 17 demonstrates that heat current decays as one increases the vibrational mismatch (measured by the ratio of Debye frequencies) between the reservoirs. We study the results for Ohmic, sub-Ohmic, and super-Ohmic environments.

B. Phonons down-conversion process

In this setup, the hot solid is kept fixed and its Debye frequency is either make equal or higher than the cutoff frequency of the cold bath. As a matter of fact the high frequency modes can not cross the system in the harmonic limit. For this set up the phonons splitting of low frequency modes are useful for transport. One may find that the heat current decays as the vibrational mismatch between the solids increases. One may further test the reaction of the cutoff frequency of the SC baths on the heat current. If we choose SC baths at a low cutoff frequency, their ability to scatter phonons reduces and as a result it approaches the harmonic limit. On the other hand, when the SC baths cover the full spectra ($\omega_{d,I}$

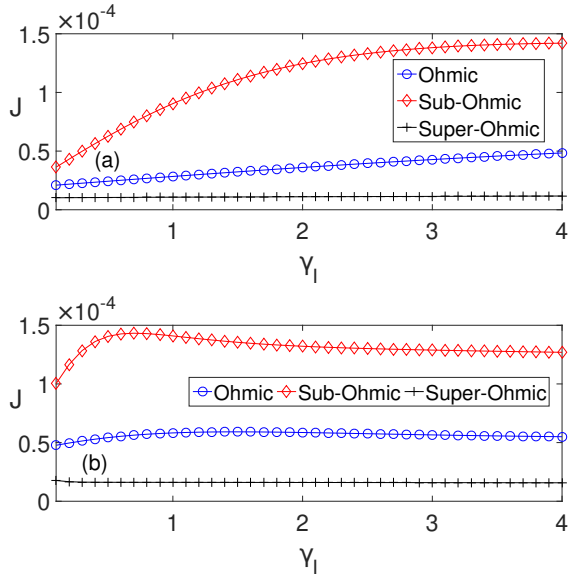


FIG. 15: Heat current as a function of phonon scattering rate at low temperatures for (a) $N = 5$ and (b) $N = 10$. In both the cases we use the QSCR method for Ohmic (o), sub-Ohmic (\diamond), and super-Ohmic (+) environments. The mismatch between the hot and cold bath is high, $\omega_{d,L}/\omega_{d,R} = 10$. $\beta_1 = 2, \beta_N = 4, \gamma_L = \gamma_R = 0.2, \omega_{d,L} = 1, \omega_{d,R} = 0.1, \omega_{d,I} = 0.1$. Here $\beta \equiv 1/T$ is the inverse temperature, $\Delta T = 0.25$, $T_a = 0.375$.

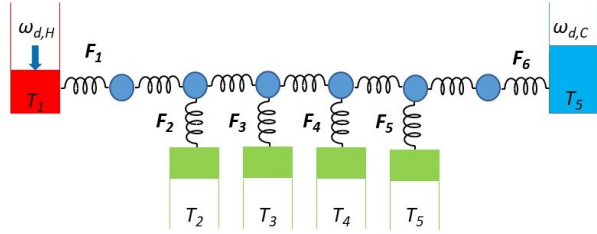


FIG. 16: Scheme of the SC model of length $N = 6$ with mismatched reservoirs for phonons up-conversion process.

large), the heat current reduces as the thermal resistance increases. In this process the SC baths basically dampen the heat current (see Fig. 19).

VI. CONCLUSIONS

It is a very much testing experience to simulate quantum heat transport and it is successfully displayed in the present paper using QSCR. Most of the anticipated results of heat transport in molecular junctions can be captured using this phenomenological QSCR. The dependence of the heat transfer on the chain length, scattering rate, and temperature are correctly emulated through this QSCR. Since this method can generate easily the classical and the quantum linear-response

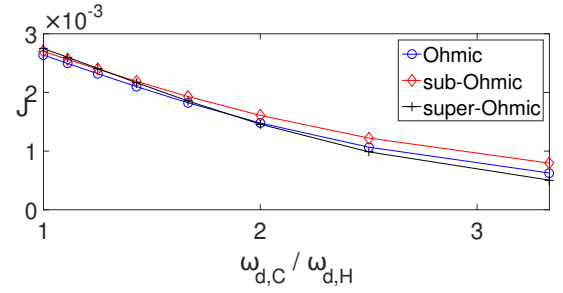


FIG. 17: Heat current as a function of phonon mismatch with mismatched reservoirs, $\omega_{d,H} = 1, 0.9, \dots, 0.3, \omega_{d,C} = 1, \omega_{d,I} = 2$ and $N = 6, \beta_1 = 2, \beta_N = 4, \gamma_L = \gamma_R = 0.2, \gamma_I = 0.8$. Here $\beta \equiv 1/T$ is the inverse temperature, $\Delta T = 0.25$, $T_a = 0.375$. Here we the results of Ohmic (o), sub-Ohmic (\diamond), and super-Ohmic (+) environments.

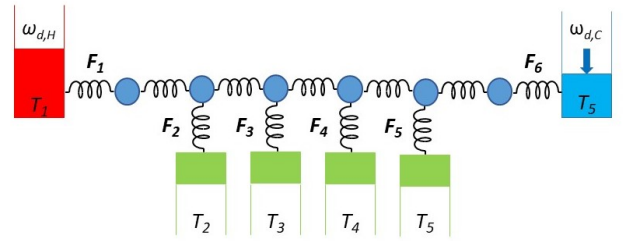


FIG. 18: Scheme of the SC model of length $N = 6$ with mismatched reservoirs for phonons down-conversion process.

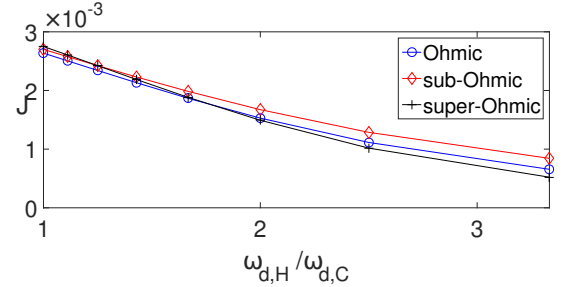


FIG. 19: Heat current as a function of phonon mismatch with mismatched reservoirs, $\omega_{d,C} = 1, 0.9, \dots, 0.3, \omega_{d,H} = 1, \omega_{d,I} = 2$ and $N = 6, \beta_1 = 2, \beta_N = 4, \gamma_L = \gamma_R = 0.2, \gamma_I = 0.8$. Here $\beta \equiv 1/T$ is the inverse temperature, $\Delta T = 0.25$, $T_a = 0.375$. Here we the results of Ohmic (o), sub-Ohmic (\diamond), and super-Ohmic (+) environments.

limits, one can use this method as a testing bed to interpolate between the ballistic and diffusive regimes. Our results also handy to reproduce the out of equilibrium condition, quantum effects and anharmonicity through this simple phenomenological model.

Furthermore, the present study exhibits the effect of different environmental spectrum and the phonon mismatch on the heat transport in MJs. Experimentally observed “turnover” phenomena is correctly reproduced

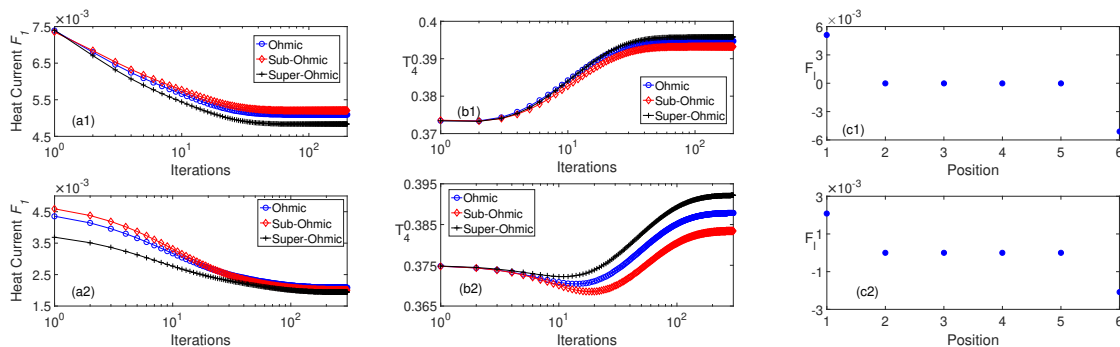


FIG. 20: Convergence of the QSCR method with the increasing number of iterations using structured bath without exponential cut-off ($\omega_d \rightarrow \infty$) baths. Top ($\gamma_I = 0.8$): (a1) net heat current, (b1) inner temperature profile for site 4, and (c1) leakage currents. Bottom ($\gamma_I = 4.0$): (a2) net heat current, (b2) inner temperature profile for site 4, and (c2) leakage currents. Parameters which are used : $N = 6$, $T_1 = 0.5$, $T_N = 0.25$, $\gamma_L = \gamma_R = 0.2$.

and the effect of different environment on such turnover effect is also demonstrated. As the QSCR is capable to reproduce the coherent to diffusive transition, one can utilize this method to study the elastic and ballistic transport in short alkane chains as well as the diffusive transport in some specific oligomers (polyethylene glycol). The in-situ local temperature evolution is helpful in study local temperature profile and the thermalization processes in MJs.

The QSCR method can be implemented to study heat transport in large disordered molecules like DNA, proteins, and amorphous polymers. Using QSCR one can go beyond one-dimension to study heat transport in realistic structures. In future one can use the QSCR method in combination with atomistic Green's function techniques to test the survival of quantum coherent effects in single-molecule phononic conductance [30,31,32].

Appendix: Numerical procedure

Numerical procedure to solve the QSCR equations are described in details in Refs. [51,53]. For completeness we review here some basics of the method discussed in Refs. [51,53]. The roots of Eq. (10) is obtained using the Newton-Raphson technique [78]. The root r of a given well-behaved function $f(x)$ satisfying $f(r) = 0$ can be obtained by iteratively solving

$$x_{k+1} = x_k - \frac{f(x_k)}{f'(x_k)}, \quad (\text{A.1})$$

where x_0 is the initial guess value and $f'(x_k)$ is the first derivative of $f(x)$ at x_k . We choose the average temperature of the system, $T_i^{(0)} = (T_1 + T_N)/2$, $i = 2, 3, \dots, N-1$, as the initial guess for the profile. The temperature of the SC reservoirs are corrected at each iteration k using

$$T_i^{(k+1)} = T_i^k - \sum_{j=2}^{N-1} (D^{-1})_{i,j} F_j(T^{(k)}). \quad (\text{A.2})$$

Here the vector $T^{(k)}$ is the temperature profile after the k th iteration and D is the Jacobian matrix with elements $D_{i,j} = \partial F_i / \partial T_j$.

To verify the convergence we examine the three quantities: (1) The temperature of the SC bath should approach a fixed value between T_1 and T_N . (2) The net heat current flowing through the system, F_1 should remain fixed. (3) Net exchange of heat current between the SC baths and chain should be vanishingly small as compared to net heat current across the system.

One can identify two major sources of error in our method: (1) we numerically integrate over frequency in Eq. (9), by discretizing energies between a lower and upper cutoffs. We ensure that considering a fine frequency step $\Delta\omega \sim 10^{-3}$ and a large energy cutoff $\omega_c \gg \omega_0$, with ω_0 as the chain characteristic frequency, our results are robust against $\Delta\omega$ and ω_c ; (2) We solve Equation (9) on a discretized temperature grid. It can be mentioned that for a coarse grid the inner reservoirs' temperatures may significantly deviate from the exact SC values, and leakage occurs [28]. We can achieve the convergence by choosing a mesh fine enough such that $|F_l|/|F_1| < 10^{-5}$ for $l = 2, 3, \dots, (N-1)$. Further, the net energy exchange between the SC baths and the system may accumulate to large values for large chain size, we also confirm in our simulations that the incoming and outgoing current, $|F_1|$ and $|F_N|$ (equal in principle), differ only by less than 0.1%. In principle, we observe that one should adopt a delicate grid for reaching a good accuracy for chains with $N > 10$. We therefore consider a two-step procedure to improve efficiency. In the first step we use a relatively rough grid with $\delta T = \frac{T_1 - T_N}{200}$, and the iterative procedure to solve Eq. (9) is followed for convergence. This is in the sense that the temperature profile stays fixed throughout the iteration procedure. However, these temperatures still deviate from the optimal (SC) temperatures, and significant leakage may take place. We denote by p the number of iterations in this part. In the second step, we develop an individual mesh around each particle site

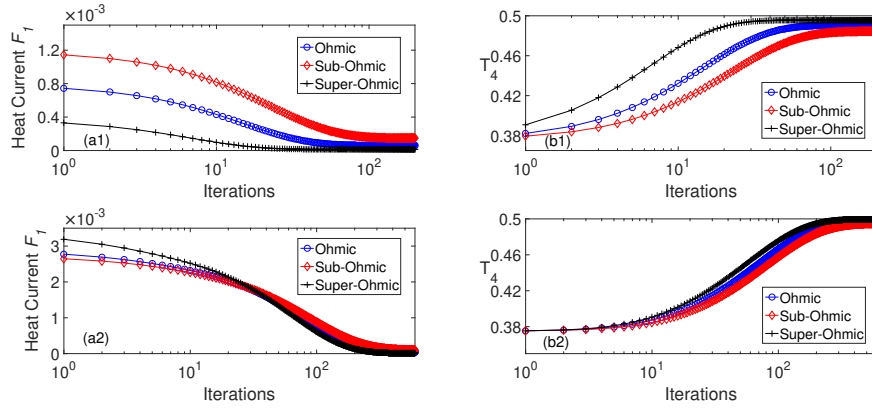


FIG. 21: Convergence of the QSCR method with the increasing number of iterations using structured baths with exponential cut-off. Top ($\omega_{d,I} = 0.1$): (a1) net heat current, and (b1) inner temperature profile for site 4. Bottom ($\omega_{d,I} = 1$): (a2) net heat current, and (b2) inner temperature profile for site 4. Parameters which are used are : $N = 6$, $T_1 = 0.5$, $T_N = 0.25$, $\gamma_L = \gamma_R = 0.2$, $\gamma_I = 4.0$, $\omega_{d,L} = 1$ and $\omega_{d,R} = 0.1$.

by considering 200 elements around temperature sector $[T_l^{(p)} - \delta T, T_l^{(p)} + \delta T]$. With this individualized grid, we further iterate Eq. (9) for q more times to achieve optimum temperature profile.

The number of iteration required to achieve convergence depends on the temperature difference, chain length, average temperature, phonon scattering rate γ_I , and the cutoff frequency ω_d . There will be more phonon scattering for large γ_I thus making convergence more challenging which is demonstrated in Fig. 20 for a chain of $N = 6$ particles. We reach convergence after 50 iterations when $\gamma_I \sim \gamma_{L,R}$. But for $\gamma_I > \gamma_{L,R}$ the convergence reached after 200 iterations. Convergence also depends on the cutoff frequency of the SC bath. If the cutoff is low then convergence can be easily reached

since only modes below cutoff frequency will suffer scattering effect. This point is illustrated in Fig. 21 where a chain of $N = 6$ particles connected to two heat baths with different cutoff frequencies. We can obtain our results for chain size $N \sim 10$ within 2-3 hours. But, it takes almost 4 days to obtain results for large chain size say $N \sim 30$.

Acknowledgments

MB acknowledges the financial support from DST through the core project CRG/2020/001768.

-
- [1] E. Scheer and J. C. Cuevas, *Molecular Electronics: An Introduction to Theory and Experiment* (World Scientific Series in Nanotechnology and Nanoscience, Singapore, 2010).
 - [2] L. Cui, R. Miao, C. Jiang, E. Meyhofer, and P. Reddy, "Perspective: Thermal and thermoelectric transport in molecular junctions," *J. Chem. Phys.* **146**, 092201 (2017).
 - [3] M. Galperin, M. A. Ratner, and A. Nitzan, "Molecular transport junctions: Vibrational effects," *J. Phys.: Condens. Matter* **19**, 103201 (2007).
 - [4] Y. Dubi and M. Di Ventra, "Colloquium: Heat flow and thermoelectricity in atomic and molecular junctions," *Rev. Mod. Phys.* **83**, 131 (2011).
 - [5] N. Li, J. Ren, L. Wang, G. Zhang, P. Hänggi, and B. Li, "Colloquium: Phononics: Manipulating heat flow with electronic analogs and beyond," *Rev. Mod. Phys.* **84**, 1045 (2012).
 - [6] D. Segal and B. K. Agarwalla, "Vibrational heat transport in molecular junctions," *Annu. Rev. Phys. Chem.* **67**, 185 (2016).
 - [7] D. G. Cahill, W. K. Ford, K. E. Goodson, G. D. Mahan, A. Majumdar, H. J. Maris, R. Merlin, and S. R. Phillpot, "Nanoscale thermal transport," *J. Appl. Phys.* **93**, 793 (2003).
 - [8] D. G. Cahill, P. V. Braun, G. Chen, D. R. Clarke, S. Fan, K. E. Goodson, P. Keblinski, W. P. King, G. D. Mahan, A. Majumdar, H. J. Maris, S. R. Phillpot, E. Pop, and L. Shi, "Nanoscale thermal transport. II. 2003–2012," *Appl. Phys. Rev.* **1**, 011305 (2014).
 - [9] T. Luo and G. Chen, "Nanoscale heat transfer—From computation to experiment," *Phys. Chem. Chem. Phys.* **15**, 3389 (2013).
 - [10] E. Pop, "Energy dissipation and transport in nanoscale devices," *Nano Res.* **3**, 147 (2010).
 - [11] T. Meier, F. Menges, P. Nirmalraj, H. Hölscher, H. Riel, and B. Gotsmann, "Length-dependent thermal transport along molecular chains," *Phys. Rev. Lett.* **113**, 060801 (2014).
 - [12] R. Y. Wang, R. A. Segalman, and A. Majumdar, "Room temperature thermal conductance of alkanedithiol self-assembled monolayers," *Appl. Phys. Lett.* **89**, 173113 (2006).

- (2006).
- [13] N. I. Rubtsova and I. V. Rubtsov, "Vibrational energy transport in molecules studied by relaxation-assisted two-dimensional infrared spectroscopy," *Annu. Rev. Phys. Chem.* **66**, 717 (2015).
- [14] D. Segal, A. Nitzan, "Heat Rectification in Molecular Junctions," *J. Chem. Phys.* **122**, 194704 (2005).
- [15] D. Segal, A. Nitzan, P. Hänggi, "Thermal Conductance through Molecular Wires," *J. Chem. Phys.* **119**, 6840 (2003).
- [16] N. Kalantar, B. K. Agarwalla, and D. Segal, "On the definitions and simulations of vibrational heat transport in nanojunctions," *J. Chem. Phys.* **153**, 174101 (2020).
- [17] A. Buldum, D. M. Leitner, S. Ciraci, "Thermal Conduction through a Molecule," *Europhys. Lett.* **47**, 208 (1999).
- [18] D. M. Leitner, "Energy Flow in Proteins," *Annu. Rev. Phys. Chem.* **59**, 233 (2008).
- [19] X.-H. Cao, W.-X. Zhou, C.-Y. Chen, L.-M. Tang, M. Long, K.-Q. Chen, "Excellent Thermoelectric Properties Induced by Different Contact Geometries in Phenalenyl-Based Single-Molecule Devices," *Sci. Rep.* **7**, 10842 (2017).
- [20] G. T. Craven, A. Nitzan, "Electron Transfer at Thermally Heterogeneous Molecule-Metal Interfaces," *J. Chem. Phys.* **146**, 092305 (2017).
- [21] G. T. Craven, A. Nitzan, "Electron Transfer across a Thermal Gradient," *Proc. Natl. Acad. Sci. U. S. A.* **113**, 9421 (2016).
- [22] R. Chen, G. T. Craven, A. Nitzan, "Electron-Transfer-Induced and Phononic Heat Transport in Molecular Environments," *J. Chem. Phys.* **147**, 124101 (2017).
- [23] Z. Qin, J. C. Bischof, "Thermophysical and Biological Responses of Gold Nanoparticle Laser Heating," *Chem. Soc. Rev.* **41**, 1191 (2012).
- [24] K. Wang, E. Meyhofer, and P. Reddy, "Thermal and thermoelectric properties of molecular junctions," *Adv. Funct. Mater.* **30**, 1904534 (2020).
- [25] A. Dhar, "Heat transport in low dimensional systems," *Adv. Phys.* **57**, 457 (2008).
- [26] N. Li, J. Ren, L. Wang, G. Zhang, P. Hänggi, and B. Li, "Colloquium: Phononics: Manipulating heat flow with electronic analogs and beyond," *Rev. Mod. Phys.* **84**, 1045 (2012).
- [27] B. C. Pein, Y. Sun, and D. D. Klott, "Unidirectional vibrational energy flow in nitrobenzene," *J. Phys. Chem. A* **117**, 6066 (2013).
- [28] B. C. Pein, Y. Sun, and D. D. Klott, "Controlling vibrational energy flow in liquid alkylbenzenes," *J. Phys. Chem. B* **117**, 10898 (2013).
- [29] N. Mingo, "Green's function methods for phonon transport through nanocontacts," in *Thermal Nanosystems and Nanomaterials*, Volume **118** of *Topics in Applied Physics*, edited by S. Volz (Springer, Berlin, Heidelberg, 2009).
- [30] D. Segal, "Heat flow in nonlinear molecular junctions: Master equation analysis," *Phys. Rev. B* **73**, 205415 (2006).
- [31] S. Lepri, R. Livi, and A. Politi, "Thermal conduction in classical low dimensional lattices," *Phys. Rep.* **377**, 1 (2003).
- [32] Y. Zhou and D. Segal, "Interface effects in thermal conduction through molecular junctions: Numerical simulations," *J. Chem. Phys.* **133**, 094101 (2010).
- [33] R. Livi, "Heat transport in one dimension," *J. Stat. Mech.* **2020**, 034001 (2020).
- [34] L. G. C. Rego and G. Kirczenow, "Quantized thermal conductance of dielectric quantum wires," *Phys. Rev. Lett.* **81**, 232 (1998).
- [35] J. C. Klöckner, J. C. Cuevas, and F. Pauly, "Transmission eigenchannels for coherent phonon transport," *Phys. Rev. B* **97**, 155432 (2018).
- [36] J. C. Klöckner, J. C. Cuevas, and F. Pauly, "Tuning the thermal conductance of molecular junctions with interference effects," *Phys. Rev. B* **96**, 245419 (2017).
- [37] J. S. Wang, B. K. Agarwalla, H. Li, and J. Thingna, "Nonequilibrium Green's function method for quantum thermal transport," *Front. Phys.* **9**, 673 (2014).
- [38] B. K. Agarwalla, J.-H. Jiang and D. Segal, "Full counting statistics of vibrationally assisted electronic conduction: Transport and fluctuations of thermoelectric efficiency," *Phys. Rev. B* **92**, 245418 (2015).
- [39] J. Thingna, J. Garcia-Palacios, and J. S. Wang, "Steady-state thermal transport in anharmonic systems: Application to molecular junctions," *Phys. Rev. B* **85**, 195452 (2012).
- [40] H. Fujisaki, L. Bu, and J. E. Straub, "Vibrational energy relaxation of a CD stretching mode in cytochrome c," *Adv. Chem. Phys.* **130B**, 179 (2005).
- [41] L.-A. Wu and D. Segal, "Quantum heat transfer: A Born-Oppenheimer method," *Phys. Rev. E* **83**, 051114 (2011).
- [42] A. Jain and J. E. Subotnik, "Vibrational energy relaxation: A benchmark for mixed quantum-classical methods," *J. Phys. Chem. A* **122**, 16 (2018).
- [43] K. Saito and T. Kato, "Kondo signature in heat transfer via a local two-state system," *Phys. Rev. Lett.* **111**, 214301 (2013).
- [44] M. Bolsterli, M. Rich, and W. M. Visscher, "Simulation of nonharmonic interactions in a crystal by self-consistent reservoirs," *Phys. Rev. A* **1**, 1086 (1970).
- [45] M. Rich and W. M. Visscher, "Disordered harmonic chain with selfconsistent reservoirs," *Phys. Rev. B* **11**, 2164 (1975).
- [46] F. Bonetto, J. L. Lebowitz, and J. Lukkarinen, "Fourier's law for a harmonic crystal with self-consistent stochastic reservoirs," *J. Stat. Phys.* **116**, 783 (2004).
- [47] F. Barros, H. C. F. Lemos, and E. Pereira, "Changing the heat conductivity: An analytical study," *Phys. Rev. E* **74**, 052102 (2006).
- [48] W. M. Visscher and M. Rich, "Stationary nonequilibrium properties of a quantum-mechanical lattice with self-consistent reservoirs," *Phys. Rev. A* **12**, 675 (1975).
- [49] A. Dhar and D. Roy, "Heat transport in harmonic lattices," *J. Stat. Phys.* **125**, 801 (2006).
- [50] D. Roy, "Crossover from ballistic to diffusive thermal transport in quantum Langevin dynamics study of a harmonic chain connected to self-consistent reservoirs," *Phys. Rev. E* **77**, 062102 (2008).
- [51] M. Bandyopadhyay and D. Segal, "Quantum heat transfer in harmonic chains with self-consistent reservoirs: Exact numerical simulations," *Phys. Rev. E* **84**, 011151 (2011).
- [52] K. Säskilähti, J. Oksanen, and J. Tulkki, "Thermal balance and quantum heat transport in nanostructures thermalized by local Langevin heat baths," *Phys. Rev. E* **88**, 012128 (2013).
- [53] R. M. Fereidani and D. Segal, "Phononic heat transport in molecular junctions : Quantum effects and vibrational

- mismatch,” J. Chem. Phys. **150**, 024105 (2019).
- [54] B. C. Pein, D. D. Dlott, “Modifying Vibrational Energy Flow in Aromatic Molecules: Effects of Ortho Substitution,” J. Phys. Chem. A **118**, 965 (2014).
- [55] A. Rajesh and M. Bandyopadhyay, Phys. Rev. A **92**, 012105 (2015); U. Weiss, *Quantum Dissipative Systems* (World Scientific, Singapore, 2008); S. Maniscalco, J. Piilo, F. Intravaia, F. Petruccione, and A. Messina, Phys. Rev. A **69**, 052101 (2004); *ibid.* **70**, 032113 (2004).
- [56] K. M. Reid, H. D. Pandey, and D. M. Leitner, J. Phys. Chem. C **123**, 6256 (2019); L. A. Pachon, and P. Brumer, J. Chem. Phys. **141**, 174102 (2014).
- [57] P. Kim, L. Shi, A. Majumdar, and P. L. McEuen, “Thermal transport measurements of individual multiwalled nanotubes,” Phys. Rev. Lett. **87**, 215502 (2001).
- [58] S. Majumdar, J. A. Sierra-Suarez, S. N. Schiffres, W. L. Ong, C. F. Higgs, A. J. McGaughey, and J. A. Malen, “Vibrational mismatch of metal leads controls thermal conductance of self-assembled monolayer junctions,” Nano Lett. **15**, 2985 (2015).
- [59] Philippe Ben-Abdallah, and Svend-Age Biehs, Phys. Rev. Lett. **112**, 044301 (2014)
- [60] Christophe Lucchesi, a Rodolphe Vaillon, and Pierre-Olivier Chapuis, Nanoscale Horizons **6**, 201 (2021)
- [61] Dakotah Thompson, Linxiao Zhu, Edgar Meyhofer, and Pramod Reddy, Nature Nanotechnology **15**, 99 (2020)
- [62] L. N. Qasim, A. Kurnosov, Y. Yue, Z. Lin, A. L. Burin, I. V. Rubtsov, “Energy Transport in PEG Oligomers: Contributions of Different Optical Bands,” J. Phys. Chem. C **120**, 26663 (2016).
- [63] J. Paavola, J. Piilo, K.-A. Suominen, and S. Maniscalco, Phys. Rev. A **79**, 052120 (2009); J. Paavola and S. Maniscalco, *ibid.* **82**, 012114 (2010).
- [64] D. Roy and A. Dhar, “Heat Transport in Ordered Harmonic Lattices,” J. Stat. Phys. **131**, 535 (2008).
- [65] M. Terraneo, M. Peyrard, and G. Casati, Phys. Rev. Lett. **88**, 094302 (2002); B. Li, L. Wang, and G. Casati, *ibid.* **93**, 184301 (2004); D. Segal and A. Nitzan, *ibid.* **94**, 034301 (2005); B. Hu, L. Yang, and Y. Zhang, *ibid.* **97**, 124302 (2006); L. A. Wu and D. Segal, *ibid.* **102**, 095503 (2009); L.-A. Wu, C. X. Yu, and D. Segal, Phys. Rev. E **80**, 041103 (2009).
- [66] E. Pereira and H. C. F. Lemos, “Symmetry of heat conductivity in inhomogeneous quantum chains,” J. Phys. A: Math. Theor. **42**, 225006 (2009).
- [67] H. Hayashi, Y. Ito and K. Takahashi, “Thermal rectification of asymmetrically-defective materials,” Journal of Mechanical Science and Technology **25**, 27 (2011).
- [68] Haidong Wang, Shiqian Hu, Koji Takahashi, Xing Zhang, Hiroshi Takamatsu, and Jie Chen, Nature Communications **8**, 15843 (2017).
- [69] M. Romero-Bastida, Jorge-Orlando Miranda-Pena, Juan M. Lopez, Phys. Rev. E **95**, 032146 (2017)
- [70] C. W. Chang, D. Okawa, A. Majumdar and A. Zettl, “SolidState Thermal Rectifier,” Science, **314**, 1121 (2006).
- [71] Mohammad Alaghemandi, F. Leroy, F. Muller-Plathe, and Michael C. Bohm, Phys. Rev. B **81**, 125410 (2010)
- [72] M Romero-Bastida and M. Ramirez-Jarquin, J. Phys. A: Math. Theor. **50**, 015004 (2017)
- [73] Yue-Yang Liu, Wu-Xing Zhou, Li-Ming Tang, and Ke-Qiu Chen, Appl. Phys. Lett. **105**, 203111 (2014).
- [74] E. Pereira, Phys. Rev. E **82**, 040101 (2010); *ibid.* **83**, 031106 (2011).
- [75] J. Wang, E. Pereira, and G. Casati, Phys. Rev. E **86**, 010101 (2012).
- [76] Nianbei Li, Jie Ren, Lei Wang, Gang Zhang, Peter Hanggi, and Baowen Li, Rev. Mod. Phys. **84**, 1045 (2012); E. T. Swartz, and R. O. Pohl, Rev. Mod. Phys. **61**, 605 (1989).
- [77] P. L. Kapitza, J. Phys. (USSR) **4**, 181 (1941).
- [78] W. H. Press, B. P. Flannery, S.A. Teukosky, and W. T. Vetterling, *Numerical Recipes in C: The Art of Scientific Computing* (Cambridge University Press, Cambridge, 1992).